Test–retest reliability of the magnetic mismatch negativity response to sound duration and omission deviants

Recasens, Marc[1], Ph.D. & Uhlhaas, Peter J.[1] Ph.D.

1. Institute of Neuroscience and Psychology, University of Glasgow, Glasgow, UK

Running title: Test–retest reliability of duration and omission MMNm
Type of manuscript: research article
Abstract: 206 words
Figures: 7
Tables: 1
Supplementary Material: 3 Tables

Corresponding Author: Dr. Peter J. Uhlhaas
Email: peter.uhlhaas@glasgow.ac.uk
Address: Institute of Neuroscience and Psychology
University of Glasgow
Hillhead Str. 58
Glasgow, G12 8QB
Phone/Fax: +44 141 330 8730

ABSTRACT

Mismatch negativity (MMN) is a neurophysiological measure of auditory novelty detection that could serve as a translational biomarker of psychiatric disorders, such as schizophrenia. However, the replicability of its magnetoencephalographic (MEG) counterpart (MMNm) has been insufficiently addressed. In the current study, test–retest reliability of the MMNm response to both duration and omission deviants was evaluated over two MEG sessions in 16 healthy adults. MMNm amplitudes and latencies were obtained at both sensor- and source-level using a cortically-constrained minimum-norm approach. Intraclass correlations (ICC) were derived to assess stability of MEG-responses over time. In addition, signal-to-noise ratios (SNR) and within-subject statistics were obtained in order to determine MMNm detectability in individual participants. ICC revealed robust values at both sensor- and source-level for both duration and omission MMNm amplitudes (ICC = 0.81–0.90), in particular in the right hemisphere, while moderate to strong values were obtained for duration MMNm and omission MMNm peak latencies (ICC = 0.74–0.88). Duration MMNm were robustly identified in individual participants with high SNR, whereas omission MMNm responses were only observed in half of the participants. Our data indicate that MMNm to unexpected duration changes and omitted sounds are highly reproducible, providing support for the use of MEG-parameters in basic and clinical research.

KEYWORDS

Magnetoencephalography (MEG); Mismatch Negativity (MMN); Event-related magnetic fields (ERF); Reliability.

1. INTRODUCTION

Mismatch Negativity (MMN) is an auditory event-related potential (ERP) component evoked by irregularities in a constant auditory stream, such as during an oddball paradigm, where responses to repetitive standard sounds are interspersed with infrequent deviants. The auditory MMN is generated in a hierarchical network involving primary and secondary auditory and frontal cortices (Doeller et al., 2003; Garrido et al., 2008; Rinne et al., 2006, 2000) and can be elicited by frequency, duration, intensity changes (Näätänen et al., 2005), and even sound omissions (Nordby et al., 1994; Yabe et al., 1998, 1997). According to the "model-adjustment hypothesis", the MMN, and its magnetoencephalographic equivalent (MMNm), result from a comparison process between sensory input and a "memory-based" perceptual model (Näätänen et al., 2005; Näätänen and Winkler, 1999). Alternatively, the "adaptation hypothesis" suggests that the MMN results from differential neural adaptation to repetitive and deviant sounds (May and Tiitinen, 2010). The predictive coding framework postulates a synthesis of these two accounts. While the MMN reflects a bottom-up prediction-error resulting from the failure to suppress top-down predictions (Garrido et al., 2009), neural adaptation could play a modulatory role by weighting the precision of prediction-errors (Auksztulewicz and Friston, 2016; Feldman and Friston, 2010).

In addition to basic research, one of the most promising roles of MMN is its use in the detection and assessment of neuropsychiatric, neurological and neurodevelopmental disorders (Näätänen et al., 2015), as well as in healthy ageing (Näätänen et al., 2012). Specifically, MMN impairments are particularly robust in schizophrenia (ScZ) (Light and Braff, 2005; Näätänen and Kähkönen, 2009; Umbricht and Krljes, 2005) and could constitute a biomarker for early detection and diagnosis of the disorder (Light and Näätänen, 2013). MMN amplitude reduction in ScZ can be linked to aberrant predictive processing that could explain cognitive deficits as well as certain symptoms of the disorder, such as, hallucinations and delusions (Adams et al., 2013; Fletcher and Frith, 2009). MMN deficits in early and prodromal stages of ScZ are particularly robust to deviations in sound duration (Bodatsch et al., 2011; Nagai et al., 2013; Todd et al., 2008). However, only few studies have shown reduced sound omission responses in ScZ (Kreitschmann-Andermahr et al., 1999; Salisbury and McCathern, 2016), thought to reflect

endogenous predictive mechanisms (Arnal and Giraud, 2012; Schröger et al., 2015; Wacongne et al., 2012).

Given the potential of ERPs as biomarkers in clinical research, it is essential to investigate their psychometric properties, such as the detectability and test-retest reliability. Previous studies have assessed the reliability of MMN to duration changes in electroencephalography (EEG) (Frodl-Bauch et al., 1997; Hall et al., 2006; Joutsiniemi et al., 1998; Kathmann et al., 1999; Light et al., 2012; Pekkonen et al., 1995; Schröger et al., 2000; Tervaniemi et al., 2005, 1999). Results from these studies indicated correlations ranging between 0.37 and 0.87, indicating moderate to robust reliability for ERPs. In contrast, the robustness of the magnetic MMN is less clear. The only study so far to address this question is by Tervaniemi and colleagues (Tervaniemi et al., 2005) who examined the replicability of MMNm and reported high intra-class correlation coefficients (ICC) to duration (ICC = 0.89) and frequency (ICC = 0.86) deviants in the right hemisphere. Equivalent current dipole (ECD) models of the MMNm did not show significant differences compared to sensor-derived measures. Previous studies indicated a signal increase of source-level estimates for both ERP and oscillatory signals (Tan et al., 2016, 2015), resulting in improved reliability (Lu et al., 2007). Noteworthy, while several studies have assessed the stability of MMN to frequency, duration and intensity deviants, test-retest reliability of the omission MMN is currently unclear.

In the present study, the reliability of both duration and omission MMNm responses was examined across two MEG recordings in healthy volunteers. We employed a short-duration (15 minutes) oddball design based on a previously tested local-global paradigm (Bekinschtein et al., 2009; Chennu et al., 2016; Wacongne et al., 2011) where MMN responses to duration and omission deviants (durMMNm and omiMMNm hereafter) were examined at both MEG sensor- and source-levels. We employed a minimum-norm estimation (MNE) approach to model distributed sources. In addition, we assessed differences between sensor- and source-estimates and evaluated the stability of MMNm responses. Our findings show a distributed network underlying both duration and omission MMNm generation and provide novel evidence that MMNm responses are highly reproducible.

2. METHODS

2.1. PARTICIPANTS

We evaluated the test-retest reliability of MMNm in sixteen participants (7 males, 3 left-handed, mean age (±sd) = 25 (±3) years) over two MEG sessions (range 20–92 days; mean (±sd) = 47 (±19) days apart). Participants were recruited from the University of Glasgow School of Psychology participant pool and provided informed consent prior to the experiment. All participants reported no history of psychiatric or neurological disorders and had normal hearing levels. To control for potential influence of hormonal fluctuations, female subjects were scanned during the same phase of their menstrual cycle in both MEG sessions. The experimental protocol was approved by the University of Glasgow College of Science and Engineering Ethics Committee. No subjects were discarded due to excessive head movement (> 0.7 cm).

2.2. STIMULI AND TASK

Series of four or five sounds composed of two superimposed sine waves (440 and 880 Hz) were presented at ~70 dB SPL using an Etymotic ER-30 system (Etymotic Research, Inc. United States of America) via 6-m plastic tubes and earpieces. Standard trials comprised series of 5 identical 80-ms tones. Deviant trials comprised four identical 80-ms sounds followed by a shorter 40-ms tone. Omission trials comprised the presentation of only four 80-ms sounds. All sounds were synthesized with 5 ms rise and fall times. The stimulus onset asynchrony (SOA) between sounds was 150 ms, and each series of sounds was separated by a random silent interval of 700 to 1000 ms. Standards trials were randomly presented with a probability of 0.6, while interspersed deviant and omission trials had a probability of 0.2 each. At least one standard sequence was presented after each deviant or omission trial and all blocks started with the presentation of 3 standard trials (Fig. 1A). Overall, 360 standard, 120 deviant, and 120 omission trials were presented across 3 blocks. To promote that attention was not directed to auditory stimulation, participants were instructed to ignore auditory stimuli while performing a simple visual detection task (with 98-100% accuracy). In each trial, a letter was presented on the screen for 150 ms and participants were requested to press a button in response to the detection of target letter “X”. Visual stimuli onset was randomized between 0 and 90 ms from the onset of the first sound to avoid time-

locked interactions with auditory stimuli. Twenty visual target trials were presented in each block during standard trials only. Trials containing button responses were removed from the analysis. The experiment was performed using Presentation® software (Version 18.0, Neurobehavioral Systems, Inc., Berkeley, CA).

2.3. NEUROIMAGING ACQUISITION

MEG data were acquired using a 248-channel magnetometer system (MAGNES® 3600WH, 4D-Neuroimaging, San Diego). Head position was assessed before and after each acquisition run via five coils attached to the participant's head and were co-digitized with participants' head shape (FASTRAK®, Polhemus Inc., VT, USA) for subsequent co-registration with individual magnetic resonance imaging (MRI) (1 mm3 T1-weighted; 3D MPRAGE). The MEG touch-pad response (LUMItouch™, Photon Control Inc., BC, Canada) was sampled synchronously at 1017.25 Hz, with online 0.1 Hz high-pass filtering.

############################## FIGURE 1 (Single column) ##############################

2.4. PREPROCESSING

Sensor-level processing was performed using Fieldtrip Toolbox (Oostenveld et al., 2011; http://www.fieldtriptoolbox.org, 20150607 and 20160623 releases) functions running under Matlab (version 8.2., The MathWorks, Natick, MA). Raw MEG signals were 0.5 Hz high-pass filtered and 50 Hz power-line noise was removed using a sharp discrete Fourier transform filter. Signals recorded by the MEG reference sensors were used to reduce environmental noise using FieldTrip's *ft_denoise_pca* function. Continuous data was down-sampled to 508.6 Hz and epoched in trials of 1.5 sec length (300 ms pre-stimulus) time-locked to the onset of the first sound in the sequence. Five excessively noisy or flat sensors were discarded from all analyses. Trials contaminated by squid jumps and amplitude ranges above ±7pT were removed prior to independent component analysis decomposition (ICA; using the "runica" algorithm as implemented in FieldTrip). Independent components containing blinks, eye movements, and cardiac activity were projected out from the data. Resulting signals were visually inspected and epochs containing amplitude ranges above ±3pT were removed. Discarded sensors were replaced using a spherical spline interpolation method. This process yielded an average (±sd) of 263.75 (±21.9) trials in the standard condition, 107.5 (±8.33) trials in the duration deviant condition and 106 (±8.43) trials in the omission condition.

Trials were bandpass filtered between 1-30 Hz (two-pass Butterworth) and baseline corrected using the 300 ms interval before the onset of the first sound in the sequence. Planar gradient transformations of the magnetometer-recorded data were calculated by taking for each sensor the average of the absolute values of the first spatial derivatives in two orthogonal directions (Bastiaansen and Knösche, 2000). Planar-transformed data projects a single positive field extrema right above the source, thus simplifying the interpretation and reducing the dimensionality of sensor-level signals. The durMMNm was computed by subtracting the waveform to the standard from the waveform to the duration deviants. Similarly, the omiMMNm was computed by subtracting the waveform to the standard from the waveform to the omission sequences. Latencies of durMMNm and omiMMNm are expressed in relation to the onset of the duration change (640 ms) and omission (600 ms) respectively, rather than to the onset of the sound sequence throughout the manuscript.

2.5. SOURCE ESTIMATION

We used an anatomically constrained approach that confined sources to the cortical mantle (Dale et al., 2000). Precise co-registration of MEG and structural MRI data was accomplished using a semiautomatic procedure. Landmark (nasion, and the 2 peri-auricular points) information was used for a first alignment of the MEG and MRI coordinate systems. The digitized head shape and the scalp surface of each individual were then used to reduce the minimum distance error between them in an iterative process. Cortical surfaces were created for each individual subject by automatically segmenting the T1-weighted MRIs into grey and white matter (GM/WM) and defining the border between GM/WM as the cortical surface. Subsequent tessellation and inflation of the folded surface patterns was carried out using Freesurfer (Dale et al., 1999; Fischl et al., 1999a; http://surfer.nmr.mgh.harvard.edu). Each individual inflated cortical surface was subsampled to ~7500 dipole locations per hemisphere, equivalent to ~5 mm spacing as the solution space for the estimated current generators. The forward model was computed in Brainstorm (Tadel et al., 2011; http://neuroimage.usc.edu/brainstorm) using an overlapping-sphere analytical model. The activation at each latency and dipole (constrained orientation) was estimated at the trial level using a noise-sensitivity normalized MNE solution known as dynamic statistic parametrical mapping (dSPM). In contrast to sensor-level analysis, the same amount of source-trials from each condition and run was randomly selected to compute source-averages. Source estimates from each individual were aligned by morphing each participant's brain to a common average cortical template (fsaverage), using a spherical morphing procedure that allowed for highly accurate inter-subject averaging (Fischl et al., 1999b). Finally, a Gaussian smoothing kernel of 3 mm full-width half-maximum (FWHM) was applied.

2.6. STATISTICAL ANALYSES

Condition-effects were assessed at both sensor- and source-level using a nonparametric cluster-based permutation approach as implemented in FieldTrip (Maris and Oostenveld, 2007). Pairwise comparisons between deviant and standard conditions for the durMMNm and between omission and standard for the omiMMNm were computed using a Monte-Carlo randomization method.

At sensor-level, statistical tests were computed on time-averaged planar-transformed data. Windows of interest were defined based on grand-average peaks: durMMNm (120–140 ms after the onset of the duration change) and omiMMNm (40–60 and 110–130 ms after the omission onset). We used 3000 permutations for bootstrapping and assumed significant condition differences when the computed p-value was smaller than the critical alpha-level of 0.05. Cluster-statistic threshold was set at $p < 0.001$ for durMMNm and $p < 0.05$ for omiMMNm. A more stringent cluster-statistic threshold was used for durMMNm as compared to omiMMNm in order to obtain physiologically plausible local clusters in both hemispheres. Clusters were obtained by summing up *t*-values from adjacent sensors and a minimum cluster of 2 adjacent sensors was required before a cluster of sensors was accepted as different between both conditions. This approach addresses the multiple comparisons problem since the test statistic is computed using all clustered values at the same time.

At the source-level, we used 1000 permutations to test for durMMNm effects between 60 and 160 ms, and omiMMNm effects between 20 to 120 ms. Cluster-statistic threshold was set at $p < 0.001$ for durMMNm and $p < 0.05$ for omiMMNm. Unlike sensor-level statistical analysis, we maintained the temporal dimension to assess the existence of significant effects in time and space. Therefore, selected samples were clustered on the basis of both spatial and temporal adjacency. Cortical dipoles were considered to be neighbours if their distance was less than 12 mm. A sample was only included into the cluster when there were at least two neighbouring samples in space or time. Using the same approach as outlined above, session-related effects were assessed statistically using pairwise comparisons between sessions independently for durMMNm and omiMMNm at sensor- and source-level.

Presence of MMNm effects at the single-subject level was assessed statistically in source-space using a non-parametric permutation method. Differences in whole-brain activity were computed between the same number of deviant and standard trials for durMMNm and between the same number of omission and standard trials for omiMMNm. Trial activity was averaged in 30 ms windows around individual peak latencies and 1000 permutation independent t-tests were used. We assumed significant condition differences when the computed p-values were smaller than the critical alpha-level of 0.05 (FDR corrected).

2.7. INDIVIDUAL PEAK AMPLITUDE AND LATENCY ESTIMATION

Individual peak amplitudes and latencies were automatically extracted using a peak detection algorithm. In order to account for inter-individual variability in peak latencies we defined search windows between 60-160 ms for the durMMNm, and between 40-140 ms for the omiMMNm, based on inspection of individual data. For planar-transformed sensor-level data twenty-four sensors of interest (SOI) located over auditory regions were used to retrieve data across subjects (Fig.1B). Peak latencies, defined as the time point with highest amplitude and surrounded by samples of smaller amplitude, were derived from averaged data across SOI in left and right hemispheres separately. Amplitudes were defined as the maximum value at the time of the peak latency. Selection of the individual peak latencies (Fig. 2) was biased to those peaks corresponding to event-related field (ERF) responses with a typical MMNm scalp topography (in non-transformed axial configuration), that is, showing an N1m hemisphere-reversed bipolar field distribution.

Individual peak amplitudes and latencies at the source-level were retrieved using the same approach and search windows as for the sensor-level data. Activity was derived from voxels within regions of interest (ROIs) overlapping bilateral auditory cortices (Fig.1C). These ROIs were manually defined by creating an 11.02-11.72 cm^2 patch (containing 112-114 cortical vertices) encompassing group-level durMMNm and omiMMNm peak voxels in each session and hemisphere. Peak estimates were extracted averaging voxels from each hemisphere-ROI separately.

2.8. TEST-RETEST RELIABILITY

We calculated ICC-values (Shrout and Fleiss, 1979) to assess the degree of relative consistency among measurements in each session. ICC is calculated as the ratio between between-subject variance and the total variance across all measures and participants. Unlike Pearson's correlation coefficient which measures the strength of the linear association between two measures, ICC takes into account the variability of the total sample and reflects the agreement of measures obtained across sessions. An ICC value of 1 indicates perfect within-subject reliability while an ICC of 0 indicates no reliability. ICC were assessed for both sensor- and source-derived durMMNm and omiMMNm amplitude and latency signals.

2.9. ESTIMATION OF INDIVIDUAL PEAK VOXELS LOCATION

For each session and participant peak voxels were identified within bilateral ROIs (~15cm^2 extended ROIs presented in Fig.1C) to ensure that local maxima within auditory areas were selected. ROIs overlaid aspects of the superior temporal gyri (STG), Heschl's gyri (HG), planum temporale (PT) and posterior aspects of the right insula. Individual peaks were drawn from source activity between 60–180 ms for durMMNm and between 20–140 ms for omiMMNm. Tables S2 and S3 (in supplementary material) describe individual peak voxel MNI coordinates, corresponding anatomical regions as extracted from the Destrieux atlas (Destrieux et al., 2010), peak amplitudes, and peak latencies. Euclidean distances between individual durMMNm and omiMMNm peak voxels in each session were calculated. Pairwise comparisons were conducted between peak voxel coordinates (X, Y, Z) to test for location differences across sessions (Session1 vs Session2), as well as differences in the location of peak voxels across conditions (durMMNm vs omiMMNm).

2.10. SIGNAL-TO-NOISE RATIO

Given that previous studies suggested that source analysis may yield more robust estimates of MEG-activity compared to sensor-derived measures (Tan et al., 2016, 2015), we computed the SNR of durMMNm and omiMMNm at both source- and sensor-levels using time-courses obtained from the above-mentioned auditory ROIs and SOIs, respectively. As in previous studies (Leue et al., 2013; Marco-Pallares et al., 2011) mean amplitudes around individual peaks (18 ms window) were divided by standard deviation of the baseline-activity (-300 to 0 ms prior to sound sequence onset). Sensor- and source-space SNR estimates of the durMMNm and omiMMNm were compared using a dependent samples t-test analysis. Measures of SNR were additionally used to compare differences in baseline-levels or signal strength between durMMNm and omiMMNm in source-space. A 2x2x2 ANOVA with factors condition (durMMNm and omiMMNm), hemispheres and sessions was used to assess significant differences in SNR in the source-space.

############################## FIGURE 2 (Double column) ##############################

3. RESULTS

3.1. SENSOR-LEVEL MMNm EFFECTS

Visual inspection of grand-averaged planar-transformed ERFs from auditory sensors of interest revealed a peak latency of durMMNm at 132 ms (Fig. 3A-B). The omiMMNm response showed two peaks between 50–56 ms and between 115–120 ms. Field distributions of axial data at peak latencies revealed topographies consistent with MMNm responses over auditory regions bilaterally (Fig. 3C-D). Cluster-based non-parametric statistics on planar-transformed ERFs showed increased responses to deviant sounds as compared to standards (120–140 ms) (Fig. 3E-F). Session1 durMMNm showed two significant clusters of sensors in right temporal-frontal regions (T_{sum} = 191.2, $P < 0.001$) and right parietal sensors (T_{sum} = 14.1, $P < 0.01$). In session 2 durMMNm showed 4 different clusters overlapping sensors in the right hemisphere (T_{sum} = 449, $P < 0.001$), left frontal regions (T_{sum} = 52.8, $P < 0.005$), left parietal (T_{sum} = 34.6, $P < 0.01$), and left auditory sensors (T_{sum} = 17.9, $P < 0.01$).

Increased responses to sound omissions as compared to standard sounds were observed (40–60 ms). In sessions 1 omiMMNm showed 2 clusters of sensors overlapping temporal-frontal bilaterally (T_{sum} = 294, $P < 0.001$), and occipital sensors (T_{sum} = 63.9, $P < 0.05$). In session 2 one single cluster overlapped bilateral temporal-frontal sensors (T_{sum} = 338.7, $P < 0.001$). It is worth noting that the early omiMMNm showed a field distribution consistent with a typical MMN, response despite of its earlier latency. During the late omiMMNm interval between 110 to 130 ms, one cluster of sensors showed increased responses to omitted sounds over midline and left hemisphere sensors in session 1 (T_{sum} = 120.2, $P < 0.005$), and session 2 (T_{sum} = 200.8, $P < 0.001$).

############################## FIGURE 3 (1.5 column) ##############################

3.2. SOURCE-LEVEL MMNm EFFECTS

Group dSPM estimates of both durMMNm and omiMMNm responses showed global maxima in auditory regions (Fig. 4C-D). Duration MMNm showed peak responses between 130 and 138 in session

1 and 2 (Fig. 4A-B), with a peak voxel located in the anterior aspect of the right STG (MNI coordinates: 54, -28, 12) and right HG (MNI coordinates: 47, -20, 11), respectively. In the left HG, durMMNm activity was ~50% weaker than in the right hemisphere. During both sessions, omiMMNm showed largest responses between 107 and 113 ms located in the right STG (MNI session 1: 46, -32, 14; MNI session 2: 59, -31, 15). Omission responses between 40 and 60 ms in both sessions were localized in anterior aspects of right STG (MNI: 54, -22, 9) and HG (MNI: 47, -20, 11). As for durMMNm, omiMMNm were ~30% smaller in the left hemisphere and located in HG and anterior aspects of the STG in both sessions. Results from cluster-based non-parametric analysis are summarized in Table 1 using the Desikan-Killiany Atlas parcellation (Fig. 4E-F).

############################## FIGURE 4 (1.5 column) ##############################

################################### TABLE 1 ###################################

3.3. INDIVIDUAL PEAK VOXEL LOCALIZATION

Pairwise t-tests comparing individual peak voxel locations across conditions did not yield significant differences in any coordinate axis (Table S1 in supplementary material). Similarly, comparison of durMMNm and omiMMNm individual peak voxel locations did not reveal significant differences, thus suggesting that both durMMNm and omiMMNm share similar underlying anatomical generators in auditory cortex. The mean (±sd) intra-participant spatial variability of peak voxel location revealed by Euclidean distances of individual peak voxels between sessions was 8.3 mm (±7.3) for durMMNm (Supp. Material: Table S2) and 12.7 mm (±10.5) for omiMMNm (Supp. Material: Table S3), suggesting a weak spatial intra-individual variability in both conditions.

############################## FIGURE 5 (1.5 column) ##############################

3.4. SIGNAL-TO-NOISE RATIO

Pairwise comparison of SNR values extracted from sensor- and source-space were performed for both durMMNm and omiMMNm responses, separately for each session and hemisphere estimates. Student’s

t-test comparisons between SNR yielded no statistically significant differences between sensor- and source-level derived measures ($p > 0.05$). Results from 2x2x2 ANOVA comparing SNR across MMNm effects, hemispheres and sessions revealed a main effect of condition, with higher SNR values for durMMNm as compared to omiMMNm ($F_{1,15} = 34.45$, $p < 0.00005$, $\eta^2 = 0.7$), and a condition x hemisphere interaction ($F_{1,15} = 5.58$, $p = 0.032$, $\eta^2 = 0.27$). Post-hoc analyses revealed increased SNR for durMMNm in the right as compared to the left hemisphere ($t_{31} = 3.07$, $p = 0.004$, $\eta^2 = 0.23$) (Fig. 7).

############################## FIGURE 6 (Single column) ##############################

3.5. INDIVIDUAL SOURCE-LEVEL MMNm EFFECTS

Results from permutation tests across trials revealed the presence of MMNm effects at the individual level (Figure 2). Statistically significant durMMNm was obtained in 10 and 12 participants in session 1 and 2 over temporal areas ($p < 0.05$, FDR corr.). One participant during session 1 and two participants during session 2 showed statistically significant effects that did not survived multiple comparisons correction ($p < 0.05$, uncorr.). In contrast, only 5 participants in both sessions showed significant omiMMNm responses ($p < 0.05$, FDR corr.). Two and three participants in session 1 and 2, respectively, showed effects that not survived statistical correction ($p < 0.05$, uncorr.) but pointed to an origin in auditory cortices.

3.6. SENSOR-LEVEL TEST-RETEST RELIABILITY

ICC for durMMNm amplitudes at sensor-level were robust over both hemispheres (right hemisphere: ICC = 0.803; $p = 0.0001$; left hemisphere: ICC = 0.796; $p = 0.0001$) (Fig. 5A). At source-level, durMMNm amplitudes showed stronger reliability in right hemisphere (right hemisphere: ICC = 0.871; $p < 0.0001$; left hemisphere: ICC = 0.676; $p = 0.001$) (Fig. 5E).

ICC indicated overall moderate to strong values for durMMNm peak latencies, both at sensor- (right hemisphere: ICC = 0.510; $p = 0.018$; left hemisphere: ICC = 0.761; $p = 0.0002$) and source-level (right hemisphere: ICC = 0.428; $p = 0.043$; left hemisphere: ICC = 0.746; $p = 0.0002$) (Fig. 5C, G).

ICC for omiMMNm amplitudes showed the strongest test-retest reliability over right hemisphere sensors (right hemisphere: ICC = 0.818; $p < 0.0001$; left hemisphere: ICC = 0.656; $p = 0.002$) (Fig. 5B). Similarly, ICC values were robust for omiMMNm amplitudes drawn from right hemisphere voxels (right hemisphere: ICC = 0.9; $p < 0.0001$; left hemisphere: ICC = 0.717; $p = 0.0006$) (Fig. 5F). OmiMMNm peak latencies obtained at both sensor- and source-level showed more robust ICC values in the right than left hemisphere (Sensor-level right hemisphere: in ICC = 0.879; $p < 0.0001$; left hemisphere: ICC = 0.633; $p = 0.003$; Source-level; right hemisphere: ICC = 0.881; $p < 0.0001$; left hemisphere: ICC = 0.717; $p = 0.0006$) (Fig. 5D,H).

############################## FIGURE 7 (Double column) ##############################

4. DISCUSSION

The current study investigated the test-retest reliability of sensor and source-reconstructed MMNm responses, indicating that both duration and omission MMNm originate from a distributed network encompassing auditory and frontal regions. Specifically, our data demonstrating highly reproducible neuromagnetic sensor- and source-MMNm estimates to both duration and omission deviants. Our findings suggest that reliable duration MMNm responses can be obtained at the individual level, thus underscoring its suitability for clinical applications. We also demonstrate that SNRs are similar for sensor-level compared to source-reconstructed estimates of both durMMNm and omiMMNm.

Consistent with prior findings (Jacobsen and Schröger, 2003; Tervaniemi et al., 1999), MMNm emerged ~130 ms after the onset of duration deviants, while omission MMNm was elicited between 50-120 ms (Bendixen et al., 2009; Salisbury, 2012; Tervaniemi et al., 1994; Wacongne et al., 2011; Yabe et al., 1998). According to predictive coding models, the MMN is thought to reflect the prediction and prediction-error response that occurs when the input differs from the predictions (Garrido et al., 2009; Lieder et al., 2013; Wacongne et al., 2011). A critical test of the predictive coding account is the MMN-response to unexpected omissions of an input, which should only reflect endogenous neural activity associated to the violation of the internal model of an upcoming event (SanMiguel et al., 2013; Schröger et al., 2015). Omission responses observed in our study are consistent with those obtained by Wacongne and colleagues (2011) showing increased responses to unexpected as compared to expected sound omission. Furthermore, we show sources of omission MMNm in frontal regions which are difficult to reconcile with neural adaptation or oscillatory rebound effects (May and Tiitinen, 2010), thus suggesting the involvement of predictive top-down mechanisms.

Source modelling across the entire cortical mantle revealed generators of duration and early omission MMNm localized in temporal areas like HG, STG, and MTG, predominantly in the right hemisphere (Mathiak et al., 2002; Mustovic et al., 2003; Rinne et al., 2005; Yabe et al., 1998), suggesting that duration and omission MMNm shared partially overlapping generators in the auditory cortex. Additional generators for both duration and late omission MMNm responses were found in a distributed network involving frontal and parietal regions (Molholm et al., 2005; Rinne et al., 2005), supporting the notion that distributed networks underlie the generation of MMNm (Wacongne et al., 2011). Beyond

auditory regions, however, a distinct pattern of sources emerged. Omission MMNm showed contributions from cingulate regions, whereas duration MMNm was characterized by the involvement of ventro-medial prefrontal and para-hippocampal areas (Rosburg et al., 2007). Accordingly, these data suggest that both MMNm responses engage overlapping but also distinct networks, pointing to potentially different computational mechanisms underlying the generation of omission and duration MMNm-responses (Wacongne et al., 2012).

ICC analyses revealed very reliable duration MMNm amplitudes across sessions. Peak latencies were characterized by slightly lower ICC-values. Our MMNm ICC-data are comparable to previous EEG studies, showing ICC scores between 0.65 and 0.87 for duration MMN amplitudes (Frodl-Bauch et al., 1997; Kathmann et al., 1999; Pekkonen et al., 1995) and MEG-findings by Tervaniemi et al. (2005). Moreover, our results obtained using a MNE distributed model corroborate that duration MMNm responses are mainly generated in the right hemisphere, showing very stable MMNm responses across assessments (Frodl-Bauch et al., 1997; Tervaniemi et al., 2005).

In addition to duration MMNm, we also assessed the test-retest reliability of MMNm to sound omissions. ICC analyses for the omission MMNm revealed very robust test-retest stability for and for latency measurements. Despite its strong replicability, omission MMNm could be identified in only half of the participants and showed significantly lower SNRs than duration MMNm-responses. Source reconstruction allowed us to estimate Euclidean distances of individual peak voxel locations across sessions, indicating a stronger stability of duration MMNm as compared to omission MMNm generators in auditory cortices.

Our findings suggest that the MMNm is reliable measure with the potential to be used as a predictor of psychosis onset (Näätänen et al., 2015). This is an important finding as MEG is increasingly used in basic and clinical neuroscience as a tool for the identification of biomarkers. It is worth noting that while previous studies have reported that source reconstruction improved SNR of auditory-steady-state (Tan et al., 2015), visual gamma responses (Tan et al., 2016), and the reliability of the auditory evoked P50 component (Lu et al., 2007), this advantage was not observed in the current study (see also: Tervaniemi et al., 2005). Thus, these data highlight that MMNm might not necessarily benefit from the use of source-derived estimates to improve SNR. Although speculative, one explanation is that

tangentially-oriented MMNm sources might be optimally detected by MEG sensors, with a low contribution from additional sources or background noise. Nevertheless, the implementation of source-reconstruction techniques allows for the accurate identification of neural generators that can alleviate differences in head position across repeated MEG runs. Future research should focus on whether SNR and individual detectability can be improved by manipulating acquisition parameters like active attention conditions (Chouiter et al., 2015; Kathmann et al., 1999), using specific post-processing methods like trial-based analysis (Bishop and Hardiman, 2010), or employing experimental paradigms like multi-feature design (Näätänen et al., 2004), comparable to ours and designed to maximize the number of deviant stimuli (> 100) while keeping a short recording time (< 15 min).

5. CONCLUSIONS

The present study demonstrates MEG-derived measures of duration and omission MMNm are highly reproducible. This is an important finding as MEG is increasingly used in basic and clinical neuroscience as a tool for the identification of biomarkers. Our results extend the notion that the duration MMNm is highly stable over time, thus underscoring its use in longitudinal, and clinical studies. Moreover, we show for first time that omission responses can be reliably used as a measure to assess predictive processing (Schröger et al., 2015). Nonetheless, we suggest that further improvements in the acquisition of omission responses are needed in order to improve its detectability in individual participants.

6. ACKNOWLEDGEMENTS

We thank Dr Tineke Grent-'T-Jong for support in the acquisition of MEG and MRI data and implementation of the stimulation protocol.

This study was supported by a research grant from Lilly UK to Peter Uhlhaas.

7. REFERENCES

Adams, R.A., Stephan, K.E., Brown, H.R., Frith, C.D., Friston, K.J., 2013. The computational anatomy of psychosis. Front. psychiatry 4, 47. doi:10.3389/fpsyt.2013.00047

Arnal, L.H., Giraud, A.L., 2012. Cortical oscillations and sensory predictions. Trends Cogn. Sci. 16, 390–398. doi:10.1016/j.tics.2012.05.003

Auksztulewicz, R., Friston, K., 2016. Repetition suppression and its contextual determinants in predictive coding. doi:10.1016/j.cortex.2015.11.024

Bastiaansen, M.C., Knösche, T.R., 2000. Tangential derivative mapping of axial MEG applied to event-related desynchronization research. Clin. Neurophysiol. 111, 1300–1305.

Bekinschtein, T.A., Dehaene, S., Rohaut, B., Tadel, F., Cohen, L., Naccache, L., 2009. Neural signature of the conscious processing of auditory regularities. Proc. Natl. Acad. Sci. U. S. A. 106, 1672–7. doi:10.1073/pnas.0809667106

Bendixen, A., Schröger, E., Winkler, I., 2009. I Heard That Coming: Event-Related Potential Evidence for Stimulus-Driven Prediction in the Auditory System. J. Neurosci. 29, 8447–8451. doi:10.1523/JNEUROSCI.1493-09.2009

Bishop, D.V.M., Hardiman, M.J., 2010. Measurement of mismatch negativity in individuals: a study using single-trial analysis. Psychophysiology 47, 697–705. doi:10.1111/j.1469-8986.2009.00970.x

Bodatsch, M., Ruhrmann, S., Wagner, M., Müller, R., Schultze-Lutter, F., Frommann, I., Brinkmeyer, J., Gaebel, W., Maier, W., Klosterkötter, J., Brockhaus-Dumke, A., 2011. Prediction of Psychosis by Mismatch Negativity. Biol. Psychiatry 69, 959–966. doi:10.1016/j.biopsych.2010.09.057

Chennu, S., Noreika, V., Gueorguiev, D., Shtyrov, Y., Bekinschtein, T.A., Henson, R., 2016. Silent Expectations: Dynamic Causal Modeling of Cortical Prediction and Attention to Sounds That Weren't. J. Neurosci. 36, 8305–16. doi:10.1523/JNEUROSCI.1125-16.2016

Chouiter, L., Tzovara, A., Dieguez, S., Annoni, J.M., Magezi, D., De Lucia, M., Spierer, L., 2015. Experience-based Auditory Predictions Modulate Brain Activity to Silence as Do Real Sounds. J. Cogn. Neurosci. 27, 1968–1980. doi:10.1162/jocn_a_00835

436 Dale, A.M., Fischl, B., Sereno, M.I., 1999. Cortical surface-based analysis. I. Segmentation and
437 surface reconstruction. Neuroimage 9, 179–94. doi:10.1006/nimg.1998.0395
438 Dale, A.M., Liu, A.K., Fischl, B.R., Buckner, R.L., Belliveau, J.W., Lewine, J.D., Halgren, E., 2000.
439 Dynamic statistical parametric mapping: combining fMRI and MEG for high-resolution imaging
440 of cortical activity. Neuron 26, 55–67.
441 Destrieux, C., Fischl, B., Dale, A., Halgren, E., 2010. Automatic parcellation of human cortical gyri
442 and sulci using standard anatomical nomenclature. Neuroimage 53, 1–15.
443 doi:10.1016/j.neuroimage.2010.06.010
444 Doeller, C., Opitz, B., Mecklinger, A., Krick, C., Reith, W., Schröger, E., 2003. Prefrontal cortex
445 involvement in preattentive auditory deviance detection: neuroimaging and electrophysiological
446 evidence. Neuroimage 20, 1270–1282.
447 Feldman, H., Friston, K.J., 2010. Attention, Uncertainty, and Free-Energy. Front. Hum. Neurosci. 4,
448 215. doi:10.3389/fnhum.2010.00215
449 Fischl, B., Sereno, M.I., Dale, A.M., 1999a. Cortical surface-based analysis. II: Inflation, flattening,
450 and a surface-based coordinate system. Neuroimage 9, 195–207. doi:10.1006/nimg.1998.0396
451 Fischl, B., Sereno, M.I., Tootell, R.B., Dale, A.M., 1999b. High-resolution intersubject averaging and
452 a coordinate system for the cortical surface. Hum. Brain Mapp. 8, 272–84.
453 Fletcher, P.C., Frith, C.D., 2009. Perceiving is believing: a Bayesian approach to explaining the
454 positive symptoms of schizophrenia. Nat. Rev. Neurosci. 10, 48–58. doi:10.1038/nrn2536
455 Frodl-Bauch, T., Kathmann, N., Möller, H.J., Hegerl, U., 1997. Dipole Localization and Test-Retest
456 Reliability of Frequency and Duration Mismatch Negativity Generator Processes. Brain Topogr.
457 10, 3–8. doi:10.1023/A:1022214905452
458 Garrido, M.I., Friston, K.J., Kiebel, S.J., Stephan, K.E., Baldeweg, T., Kilner, J.M., 2008. The
459 functional anatomy of the MMN: A DCM study of the roving paradigm. Neuroimage 42, 936–
460 944. doi:10.1016/j.neuroimage.2008.05.018
461 Garrido, M.I., Kilner, J.M., Stephan, K.E., Friston, K.J., 2009. The mismatch negativity: A review of
462 underlying mechanisms. Clin. Neurophysiol. 120, 453–463. doi:10.1016/j.clinph.2008.11.029
463 Hall, M.H., Schulze, K., Rijsdijk, F., Picchioni, M., Ettinger, U., Bramon, E., Freedman, R., Murray,

R.M., Sham, P., 2006. Heritability and Reliability of P300, P50 and Duration Mismatch Negativity. Behav. Genet. 36, 845–857. doi:10.1007/s10519-006-9091-6

Jacobsen, T., Schröger, E., 2003. Measuring duration mismatch negativity. Clin. Neurophysiol. 114, 1133–43.

Joutsiniemi, S.L., Ilvonen, T., Sinkkonen, J., Huotilainen, M., Tervaniemi, M., Lehtokoski, A., Rinne, T., Näätänen, R., 1998. The mismatch negativity for duration decrement of auditory stimuli in healthy subjects. Electroencephalogr. Clin. Neurophysiol. 108, 154–9.

Kathmann, N., Frodl-Bauch, T., Hegerl, U., 1999. Stability of the mismatch negativity under different stimulus and attention conditions. Clin. Neurophysiol. 110, 317–23.

Kreitschmann-Andermahr, I., Rosburg, T., Meier, T., Volz, H.-P.P., Nowak, H., Sauer, H., 1999. Impaired sensory processing in male patients with schizophrenia—a magnetoencephalographic study of auditory mismatch detection. Schizophr. Res. 35, 121–129. doi:10.1016/S0920-9964(98)00115-7

Leue, A., Klein, C., Lange, S., Beauducel, A., 2013. Inter-individual and intra-individual variability of the N2 component: On reliability and signal-to-noise ratio. Brain Cogn. 83, 61–71. doi:10.1016/j.bandc.2013.06.009

Lieder, F., Stephan, K.E., Daunizeau, J., Garrido, M.I., Friston, K.J., 2013. A Neurocomputational Model of the Mismatch Negativity. PLoS Comput. Biol. 9, e1003288. doi:10.1371/journal.pcbi.1003288

Light, G.A., Braff, D.L., 2005. Mismatch negativity deficits are associated with poor functioning in schizophrenia patients. Arch. Gen. Psychiatry 62, 127–36. doi:10.1001/archpsyc.62.2.127

Light, G.A., Näätänen, R., 2013. Mismatch negativity is a breakthrough biomarker for understanding and treating psychotic disorders. Proc. Natl. Acad. Sci. U. S. A. 110, 15175–6. doi:10.1073/pnas.1313287110

Light, G.A., Swerdlow, N.R., Rissling, A.J., Radant, A., Sugar, C.A., Sprock, J., Pela, M., Geyer, M.A., Braff, D.L., 2012. Characterization of Neurophysiologic and Neurocognitive Biomarkers for Use in Genomic and Clinical Outcome Studies of Schizophrenia. PLoS One 7, e39434. doi:10.1371/journal.pone.0039434

Lu, B.Y., Edgar, J.C., Jones, A.P., Smith, A.K., Huang, M.-X., Miller, G.A., Cañive, J.M., 2007. Improved test-retest reliability of 50-ms paired-click auditory gating using magnetoencephalography source modeling. Psychophysiology 44, 86–90. doi:10.1111/j.1469-8986.2006.00478.x

Marco-Pallares, J., Cucurell, D., Münte, T.F., Strien, N., Rodriguez-Fornells, A., 2011. On the number of trials needed for a stable feedback-related negativity. Psychophysiology 48, 852–860. doi:10.1111/j.1469-8986.2010.01152.x

Maris, E., Oostenveld, R., 2007. Nonparametric statistical testing of EEG- and MEG-data. J. Neurosci. Methods 164, 177–190.

Mathiak, K., Rapp, A., Kircher, T., Grodd, W., Hertrich, I., Weiskopf, N., 2002. Mismatch responses to randomized gradient switching noise as reflected by fMRI and whole-head magnetoencephalography. Hum. Brain Mapp. 16, 190–195.

May, P.J.C., Tiitinen, H., 2010. Mismatch negativity (MMN), the deviance-elicited auditory deflection, explained. Psychophysiology 47, 66–122. doi:10.1111/j.1469-8986.2009.00856.x

Molholm, S., Martinez, A., Ritter, W., Javitt, D.C., Foxe, J.J., 2005. The neural circuitry of pre-attentive auditory change-detection: an fMRI study of pitch and duration mismatch negativity generators. Cereb. Cortex 15, 545–51. doi:10.1093/cercor/bhh155

Mustovic, H., Scheffler, K., Di Salle, F., Esposito, F., Neuhoff, J.G., Hennig, J., Seifritz, E., 2003. Temporal integration of sequential auditory events: silent period in sound pattern activates human planum temporale. Neuroimage 20, 429–34.

Näätänen, R., Jacobsen, T., Winkler, I., 2005. Memory-based or afferent processes in mismatch negativity (MMN): a review of the evidence. Psychophysiology 42, 25–32. doi:10.1111/j.1469-8986.2005.00256.x

Näätänen, R., Kähkönen, S., 2009. Central auditory dysfunction in schizophrenia as revealed by the mismatch negativity (MMN) and its magnetic equivalent MMNm: a review. Int. J. Neuropsychopharmacol. 12, 125–35. doi:10.1017/S1461145708009322

Näätänen, R., Kujala, T., Escera, C., Baldeweg, T., Kreegipuu, K., Carlson, S., Ponton, C., 2012. The mismatch negativity (MMN) – A unique window to disturbed central auditory processing in

ageing and different clinical conditions. Clin. Neurophysiol. 123, 424–458. doi:10.1016/j.clinph.2011.09.020

Näätänen, R., Pakarinen, S., Rinne, T., Takegata, R., 2004. The mismatch negativity (MMN): towards the optimal paradigm. Clin. Neurophysiol. 115, 140–144. doi:10.1016/j.clinph.2003.04.001

Näätänen, R., Shiga, T., Asano, S., Yabe, H., 2015. Mismatch negativity (MMN) deficiency: A break-through biomarker in predicting psychosis onset. Int. J. Psychophysiol. doi:10.1016/j.ijpsycho.2014.12.012

Näätänen, R., Winkler, I., 1999. The concept of auditory stimulus representation in cognitive neuroscience. Psychol. Bull. 125, 826–859.

Nagai, T., Tada, M., Kirihara, K., Yahata, N., Hashimoto, R., Araki, T., Kasai, K., 2013. Auditory mismatch negativity and P3a in response to duration and frequency changes in the early stages of psychosis. Schizophr. Res. 150, 547–554. doi:10.1016/j.schres.2013.08.005

Nordby, H., Hammerborg, D., Roth, W.T., Hugdahl, K., 1994. ERPs for infrequent omissions and inclusions of stimulus elements. Psychophysiology 31, 544–52.

Oostenveld, R., Fries, P., Maris, E., Schoffelen, J.-M., 2011. FieldTrip: Open source software for advanced analysis of MEG, EEG, and invasive electrophysiological data. Comput. Intell. Neurosci. 2011, 156869. doi:10.1155/2011/156869

Pekkonen, E., Rinne, T., Näätänen, R., 1995. Variability and replicability of the mismatch negativity. Electroencephalogr. Clin. Neurophysiol. 96, 546–54.

Rinne, T., Alho, K., Ilmoniemi, R.J.J., Virtanen, J., Näätänen, R., 2000. Separate time behaviors of the temporal and frontal mismatch negativity sources. Neuroimage 12, 14–9. doi:10.1006/nimg.2000.0591

Rinne, T., Degerman, A., Alho, K., 2005. Superior temporal and inferior frontal cortices are activated by infrequent sound duration decrements: An fMRI study. Neuroimage 26, 66–72.

Rinne, T., Särkkä, A., Degerman, A., Schröger, E., Alho, K., 2006. Two separate mechanisms underlie auditory change detection and involuntary control of attention. Brain Res. 1077, 135–43. doi:10.1016/j.brainres.2006.01.043

Rosburg, T., Trautner, P., Ludowig, E., Schaller, C., Kurthen, M., Elger, C.E., Boutros, N.N., 2007.

548 Hippocampal event-related potentials to tone duration deviance in a passive oddball paradigm in
549 humans. Neuroimage 37, 274–281. doi:10.1016/j.neuroimage.2007.05.002
550 Salisbury, D.F., 2012. Finding the missing stimulus mismatch negativity (MMN): Emitted MMN to
551 violations of an auditory gestalt. Psychophysiology 49, 544–548. doi:10.1111/j.1469-
552 8986.2011.01336.x
553 Salisbury, D.F., McCathern, A.G., 2016. Abnormal Complex Auditory Pattern Analysis in
554 Schizophrenia Reflected in an Absent Missing Stimulus Mismatch Negativity. Brain Topogr. 29,
555 867–874. doi:10.1007/s10548-016-0514-2
556 SanMiguel, I., Saupe, K., Schröger, E., 2013. I know what is missing here: electrophysiological
557 prediction error signals elicited by omissions of predicted ”what” but not ”when”. Front. Hum.
558 Neurosci. 7, 407. doi:10.3389/fnhum.2013.00407
559 Schröger, E., Giard, M.H., Wolff, C., 2000. Auditory distraction: event-related potential and
560 behavioral indices. Clin. Neurophysiol. 111, 1450–60.
561 Schröger, E., Marzecová, A., SanMiguel, I., 2015. Attention and prediction in human audition: a
562 lesson from cognitive psychophysiology. Eur. J. Neurosci. 41, 641–664. doi:10.1111/ejn.12816
563 Shrout, P.E., Fleiss, J.L., 1979. Intraclass correlations: Uses in assessing rater reliability. Psychol.
564 Bull. 86, 420–428. doi:10.1037/0033-2909.86.2.420
565 Tadel, F., Baillet, S., Mosher, J.C., Pantazis, D., Leahy, R.M., 2011. Brainstorm: a user-friendly
566 application for MEG/EEG analysis. Comput. Intell. Neurosci. 2011, 879716.
567 doi:10.1155/2011/879716
568 Tan, H.-R.M., Gross, J., Uhlhaas, P.J., 2016. MEG sensor and source measures of visually induced
569 gamma-band oscillations are highly reliable. Neuroimage 137, 34–44.
570 doi:10.1016/j.neuroimage.2016.05.006
571 Tan, H.-R.M., Gross, J., Uhlhaas, P.J., 2015. MEG—measured auditory steady-state oscillations show
572 high test–retest reliability: A sensor and source-space analysis. Neuroimage 122, 417–426.
573 doi:10.1016/j.neuroimage.2015.07.055
574 Tervaniemi, M., Lehtokoski, a, Sinkkonen, J., Virtanen, J., Ilmoniemi, R.J., Näätänen, R., 1999. Test-
575 retest reliability of mismatch negativity for duration, frequency and intensity changes. Clin.

Neurophysiol. 110, 1388–93.

Tervaniemi, M., Saarinen, J., Paavilainen, P., Danilova, N., Näätänen, R., 1994. Temporal integration of auditory information in sensory memory as reflected by the mismatch negativity. Biol. Psychol. 38, 157–67.

Tervaniemi, M., Sinkkonen, J., Virtanen, J., Kallio, J., Ilmoniemi, R.J., Salonen, O., Näätänen, R., 2005. Test-retest stability of the magnetic mismatch response (MMNm). Clin. Neurophysiol. 116, 1897–905. doi:10.1016/j.clinph.2005.03.025

Todd, J., Michie, P.T., Schall, U., Karayanidis, F., Yabe, H., Näätänen, R., 2008. Deviant matters: duration, frequency, and intensity deviants reveal different patterns of mismatch negativity reduction in early and late schizophrenia. Biol. Psychiatry 63, 58–64. doi:10.1016/j.biopsych.2007.02.016

Umbricht, D., Krljes, S., 2005. Mismatch negativity in schizophrenia: a meta-analysis. Schizophr. Res. 76, 1–23. doi:10.1016/j.schres.2004.12.002

Wacongne, C., Changeux, J.-P., Dehaene, S., 2012. A Neuronal Model of Predictive Coding Accounting for the Mismatch Negativity. J. Neurosci. doi:10.1523/JNEUROSCI.5003-11.2012

Wacongne, C., Labyt, E., van Wassenhove, V., Bekinschtein, T., Naccache, L., Dehaene, S., 2011. Evidence for a hierarchy of predictions and prediction errors in human cortex. Proc. Natl. Acad. Sci. U. S. A. 108, 20754–9. doi:10.1073/pnas.1117807108

Yabe, H., Tervaniemi, M., Reinikainen, K., Näätänen, R., 1997. Temporal window of integration revealed by MMN to sound omission. Neuroreport 8, 1971–4.

Yabe, H., Tervaniemi, M., Sinkkonen, J., Huotilainen, M., Ilmoniemi, R.J., Näätänen, R., 1998. Temporal window of integration of auditory information in the human brain. Psychophysiology 35, 615–9.

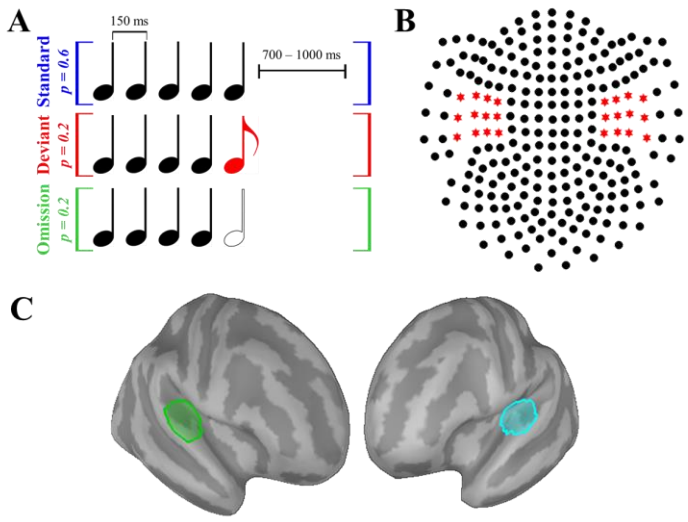

Figure 1: A) Experimental design. Standard sequences comprised five identical 80 ms tones and were presented with a probability of 0.6. Unexpected deviant sequences comprising four identical 80-ms tones followed by a 40 ms tone (highlighted in red), and omission sequences comprising four identical 80-ms tones only, were interspersed among standard sequences with a probability of 0.4 each. Inter-trial interval randomly varied between 700 and 1000 ms and stimulus-onset asynchrony was set at 150 ms. B) MEG sensor layout depicting sensors of interest highlighted in red used to derive planar-transformed event-related fields (Left hemisphere: 'A158', 'A130', 'A98', 'A157', 'A129', 'A97', 'A156', 'A128', 'A96', 'A67', 'A68', 'A69'. Right hemisphere: 'A144', 'A112', 'A81', 'A145', 'A113', 'A82', 'A146', 'A114', 'A83', 'A171', 'A172', 'A173'). C) Template cortical surface highlighting regions-of-interest used to derive time-courses of activity and individual peak voxels.

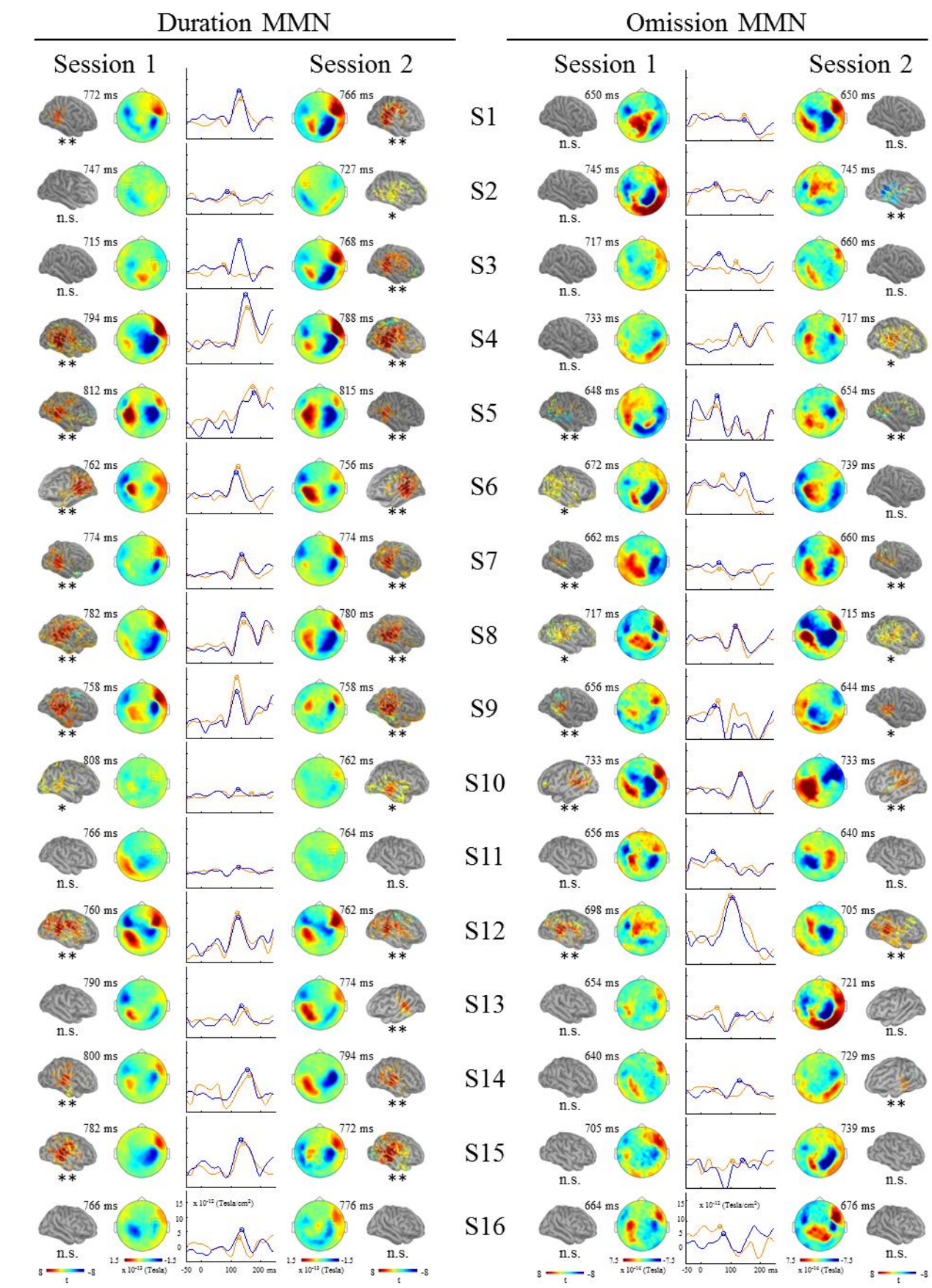

from sensors of interest. Statistical t-maps show within-subjects permutation results overlaid on individual inflated cortical surfaces. (** $p < 0.05$, FDR corrected; * $p < 0.05$, uncorrected; n.s. Not significant) at peak latency (± 15 ms). Only subject 2 (omission MMN, session 2) showed enhanced activity to standard sounds

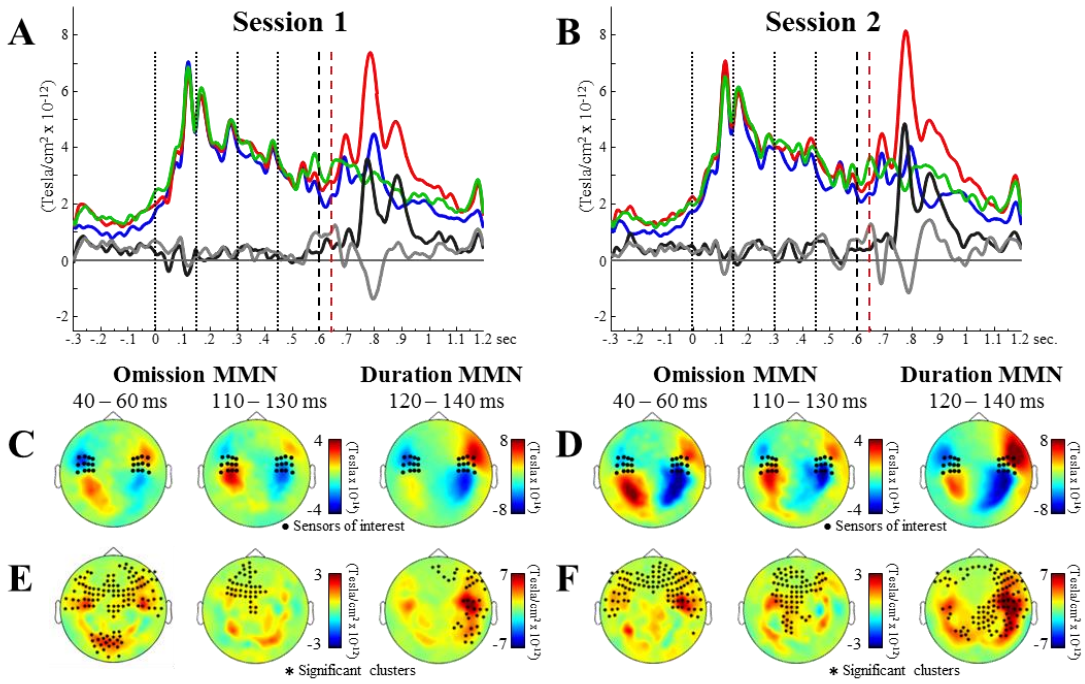

Figure 3: Sensor-level data. A-B) Grand-averaged time-courses from session 1 and 2 showing planar-transformed ERFs (Standard – blue, deviant – red, omission – green, durMMNm – black, omiMMNm - grey) derived from sensors of interest highlighted (●) on topographic maps (C and D).. Latencies are expressed with respect to the onset of the sound sequence. Dotted lines indicate stimuli onset. Dashed lines indicate onset of omission (black) and duration (red) deviants.C-D) Topographic maps from session 1 and 2 showing axial field distribution. E-F) Results from cluster-based permutation analysis overlied onto planar-transformed topographic maps during session 1 and 2. Highlighted sensors (*) show significant clusters of sensors.

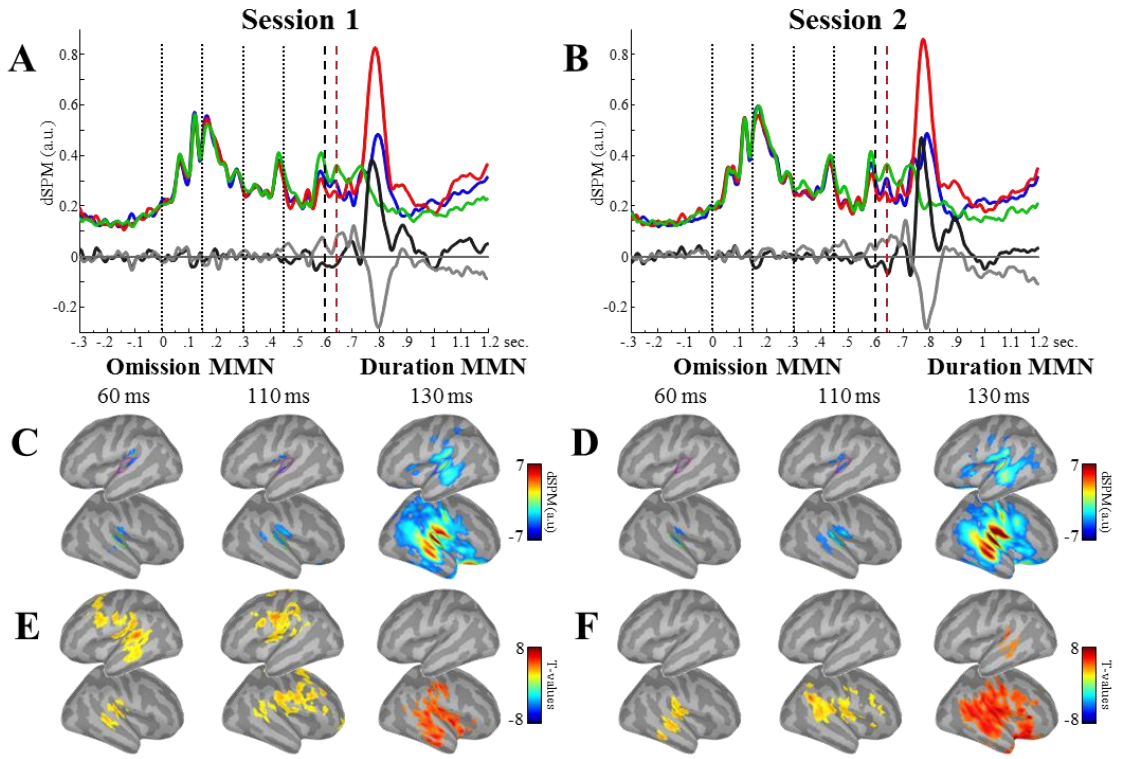

Figure 4: Source-level data. A-B) Grand-averaged dSPM time-courses from session 1 and 2 (Standard – blue, deviant – red, omission – green, durMMNm – black, omiMMNm - grey) derived from auditory ROIs highlighted in purple and green for left and right hemispheres respectively over activation maps (C and D). Dotted lines indicate stimuli onset. Dashed lines indicate onset of omission (black) and duration (red) deviants. C-D) Whole-brain activation maps from session 1 and 2 showing cortically-constrained dSPM values overlaid on a template brain (FSaverage). E-F) Results from cluster-based permutation analysis during session 1 and 2 showing significant clusters of time-samples and voxels.

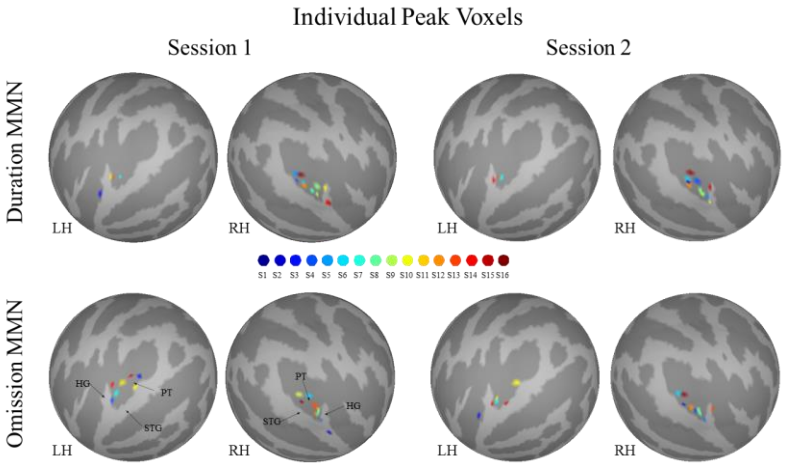

Figure 5: Individual peak voxels observed for duration and omission MMNm in session 1 and 2. Peak voxels represent local maxima as observed within extended ROIs (Fig. 1C) overlapping supratemporal regions bilaterally: HG (Heschl's gyrus), STG (superior temporal gyrus), (PT) planum temporale, and posterior insula. Peak voxels from subjects 1 (omission MMNm session 1) and 2 (duration MMNm session 1, and omission MMNm session 2) were located outside the ROI.

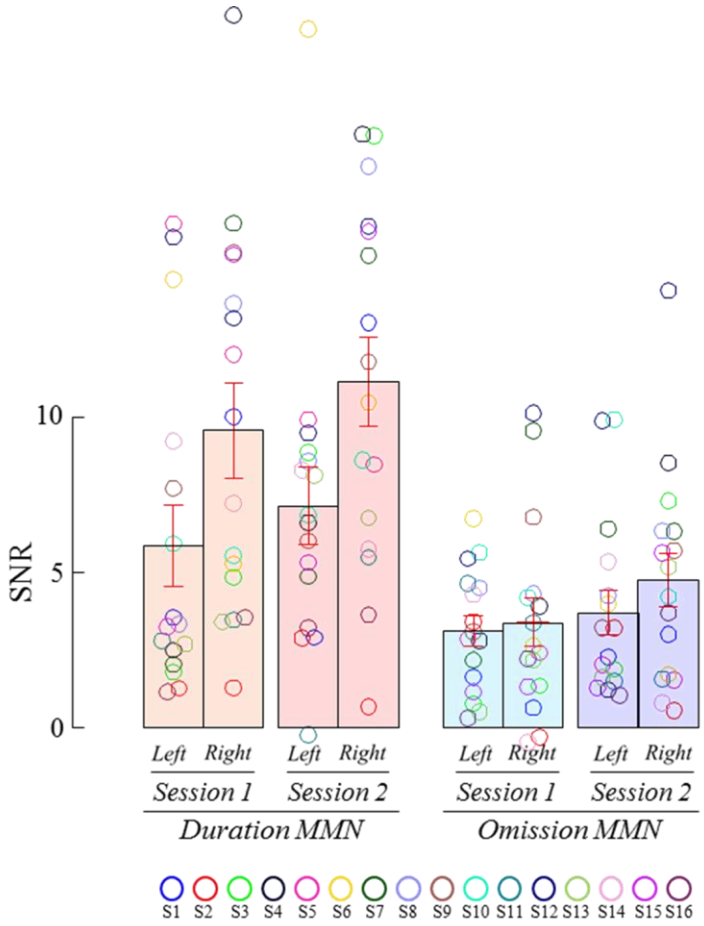

Figure 6: Bar graphs (mean; red whiskers indicate standard error of mean) and individual values for SNR estimates of duration (left) and omission (right) MMNm, in each session and hemisphere.

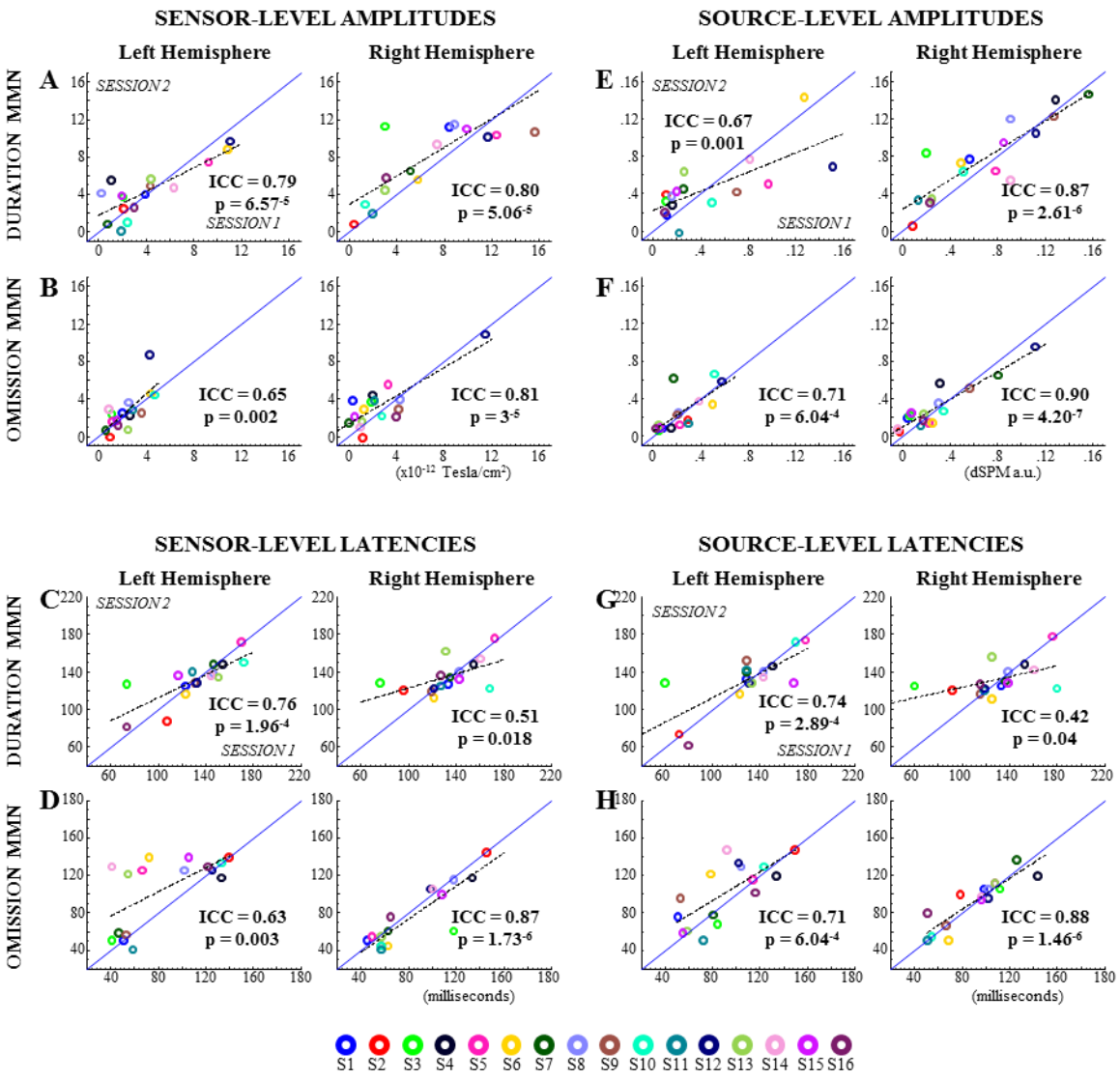

Figure 7: Summary of intraclass correlation (ICC) and individual estimates of amplitude and latency for duration and omission MMNm, in session 1 and 2, in sensor- and source-space. X-axis denotes individual values in session 1, and Y-axis in session 2. Dashed line indicates linear polynomial fit. Plots show sensor-level A) test-retest duration MMNm and B) omission MMNm amplitudes, C) test-retest duration MMNm and D) omission MMNm peak latencies; and source-level E) test-retest duration MMNm and F) omission MMNm amplitudes, G) test-retest duration MMNm and H) omission MMNm peak latencies.

	Omission MMN SESSION 1			Omission MMN SESSION 2			Duration MMN SESSION 1			Duration MMN SESSION 2		
	Latency	p-val.	Brain regions %	Latency	p-val.	Brain regions %	Latency	p-val.	Brain regions %	Latency	p-val.	Brain regions %
Clust. 1	27 - 120	0.018	'posteriorcingulate L' 92 'caudalmiddlefrontal L' 82 'paracentral L' 76 'precentral L' 71 'bankssts L' 66 'postcentral L' 66 'supramarginal L' 64 'transversetemporal L' 59 'superiortemporal L' 50 'rostralanteriorcingulate L' 48 'superiorfrontal L' 45 'precuneus L' 33 'medialorbitofrontal L' 30 'insula L' 29 'middletemporal L' 27 'parsopercularis L' 27 'caudalanteriorcingulate L' 24 'isthmuscingulate L' 22 'parstriangularis L' 13	20 - 120	0.026	'transversetemporal R' 100 'bankssts R' 95 'supramarginal R' 74 'superiortemporal R' 47 'middletemporal R' 46 'inferiorparietal R' 40 'insula R' 37 'parsopercularis R' 34 'postcentral R' 30 'parstriangularis R' 28 'caudalmiddlefrontal R' 24 'precentral R' 21 'inferiortemporal R' 11	107 – 160	0.002	'lateralorbitofrontal R' 95 'insula R' 91 'bankssts R' 85 'transversetemporal R' 79 'medialorbitofrontal R' 75 'supramarginal R' 59 'rostralanteriorcingulate R' 58 'temporalpole R' 51 'middletemporal R' 49 'parstriangularis R' 46 'parsorbitalis R' 42 'inferiortemporal R' 40 'postcentral R' 36 'superiortemporal R' 35 'entorhinal R' 34 'frontalpole R' 16 'parahippocampal R' 11	105 – 160	0.002	'transversetemporal R' 100 'bankssts R' 94 'temporalpole R' 87 'parsopercularis R' 76 'lateralorbitofrontal R' 71 'supramarginal R' 71 'superiortemporal R' 67 'insula R' 66 'middletemporal R' 55 'inferiortemporal R' 50 'parstriangularis R' 47 'postcentral R' 44 'precentral R' 33 'inferiorparietal R' 29 'entorhinal R' 22 'fusiform R' 18 'parsorbitalis R' 16 'caudalmiddlefrontal R' 15 'medialorbitofrontal R' 13
Clust. 2	20 – 120	0.02	'bankssts R' 98 'frontalpole R' 96 'paracentral R' 93 'rostralanteriorcingulate R' 76 'posteriorcingulate R' 68 'transversetemporal R' 61 'superiorfrontal R' 60 'caudalmiddlefrontal R' 57 'postcentral R' 53 'medialorbitofrontal R' 50 'parsopercularis R' 48 'rostralmiddlefrontal R' 48 'supramarginal R' 45 'precentral R' 44 'superiortemporal R' 36 'precuneus R' 25 'lateralorbitofrontal R' 23 'caudalanteriorcingulate R' 21 'middletemporal R' 21 'isthmuscingulate R' 20 'parstriangularis R' 20 'inferiorparietal R' 19 'insula R' 19				128 – 156	0.009	'medialorbitofrontal L' 40 'rostralanteriorcingulate L' 23	128 – 160	0.002	'bankssts L' 85 'superiortemporal L' 34 'supramarginal L' 29 'middletemporal L' 26
Clust. 3										755 – 776	0.03	'precuneus L' 20

Table 1: Source-level cluster-based results. Brain regions correspond to Desikan-Killiany Atlas parcelation (% overlap)

Supplementary Material

TABLE S1: Comparison of individual peak-voxels location

		P-value	T-value
Duration MMNm Sess1 vs Sess2	X-axis	0.297	1.079
	Y-axis	0.621	0.506
	Z-axis	0.790	-0.270
Omission MMNm Sess1 vs Sess2	X-axis	0.592	-0.547
	Y-axis	0.108	-1.707
	Z-axis	0.291	1.093
Session 1 Dur vs Omi MMNm	X-axis	0.219	1.281
	Y-axis	0.210	1.310
	Z-axis	0.511	-0.672
Session 2 Dur vs Omi MMNm	X-axis	0.070	-1.954
	Y-axis	0.631	-0.490
	Z-axis	0.533	0.638

TABLE S2: Duration MMNm individual peak voxels in session 1 and 2. Peak latencies are expressed with respect to the onset of the first sound in the sequence. Absolute X-axis values are used for the calculation of Euclidean distances.

DURATION MMN													
	SESSION 1						**Euclidean Distance (mm)**	**SESSION 2**					
	Anatomical Label	**MNI coordinates (mm)**			**dSPM Value (a.u.)**	**Peak Latency (sec)**		**dSPM Value (a.u.)**	**Peak Latency (sec)**	**MNI coordinates (mm)**			Anatomical Label
		x	**y**	**z**						x	y	z	
1	'G_temp_sup-Plan_tempo R'	54	-28	12	1.1695	0.7746	0	1.4686	0.7648	54	-28	12	'G_temp_sup-Plan_tempo R'
2	'G_temp_sup-G_T_transv L'	-51	-10	4	0.4050	0.7746	14	0.7608	0.8199	-51	-24	7	'G_temp_sup-G_T_transv L'
3	'G_temp_sup-Plan_tempo R'	63	-29	14	0.2424	0.7727	17	1.3805	0.7648	46	-28	11	'Lat_Fis-post R'
4	'G_temp_sup-Plan_tempo R'	55	-32	17	2.6198	0.7884	18	2.5632	0.7884	53	-16	8	'G_temp_sup-G_T_transv R'
5	'G_temp_sup-Plan_tempo R'	54	-28	12	1.9759	0.7904	4	1.2832	0.8140	52	-31	15	'G_temp_sup-Plan_tempo R'
6	'S_temporal_transverse L'	-51	-24	4	2.0726	0.7628	1	2.3586	0.7569	-51	-23	4	'S_temporal_transverse L'
7	'G_temp_sup-Plan_tempo R'	54	-22	9	2.5143	0.7786	5	2.6698	0.7687	53	-19	6	'S_temporal_transverse R'
8	'S_temporal_transverse R'	46	-26	10	1.5629	0.7746	6	2.1109	0.7786	50	-23	8	'S_temporal_transverse R'
9	'S_temporal_transverse R'	53	-20	6	2.2214	0.7569	0	2.1184	0.7589	53	-20	6	'S_temporal_transverse R'
10	'G_temp_sup-G_T_transv R'	41	-24	13	0.9076	0.8179	18	1.3056	0.7628	53	-12	7	'G_temp_sup-G_T_transv R'
11	'G_temp_sup-G_T_transv L'	-50	-24	9	0.3966	0.7687	13	0.4907	0.7923	46	-34	18	'Lat_Fis-post R'
12	'G_temp_sup-Plan_tempo R'	56	-26	11	2.5074	0.7609	0	2.0284	0.7628	56	-26	11	'G_temp_sup-Plan_tempo R'
13	'G_temp_sup-G_T_transv L'	-51	-24	7	0.5829	0.8002	0	1.0179	0.7707	-51	-24	7	'G_temp_sup-G_T_transv L'
14	'G_temp_sup-G_T_transv R'	52	-11	6	1.5086	0.7982	11	1.3762	0.7746	-51	-21	10	'G_temp_sup-G_T_transv L'
15	'G_temp_sup-G_T_transv R'	50	-10	4	1.3892	0.7805	19	1.3762	0.7668	41	-24	13	'G_temp_sup-G_T_transv R'
16	'G_temp_sup-Plan_tempo R'	52	-32	16	0.3846	0.7805	7	0.8608	0.7727	46	-34	18	'Lat_Fis-post R'

TABLE S3: Duration MMNm individual peak voxels in session 1 and 2. Peak latencies are expressed with respect to the onset of the first sound in the sequence. Absolute X-axis values are used for the calculation of Euclidean distances.

OMISSION MMN													
	SESSION 1							SESSION 2					
	Anatomical Label	MNI coordinates (mm)			dSPM Value (a.u.)	Peak Latency (sec)	Euclidean Distance (mm)	dSPM Value (a.u.)	Peak Latency (sec)	MNI coordinates (mm)			Anatomical Label
		x	y	z						x	y	z	
1	'G_temp_sup-G_T_transv R'	-48	-40	22	0.2851	0.6547	24	0.4389	0.7058	62	-26	9	'S_temporal_transverse R'
2	'Lat_Fis-post R'	-53	-38	18	0.3167	0.7117	35	0.3115	0.6744	-51	-7	1	'G_temp_sup-Plan_tempo R'
3	'S_temporal_transverse L'	67	-10	-3	0.1906	0.7196	21	0.3672	0.6567	54	-22	9	'S_temporal_transverse L'
4	'S_temporal_transverse R'	54	-14	6	0.7588	0.7392	2	1.0208	0.7176	55	-15	6	'S_temporal_transverse R'
5	'G_temp_sup-G_T_transv R'	43	-33	15	1.0010	0.7058	12	0.7625	0.7098	55	-32	17	'S_temporal_transverse R'
6	'G_temp_sup-Plan_tempo R'	-46	-28	6	1.0459	0.6803	10	0.6785	0.7216	-53	-21	4	'G_temp_sup-Plan_tempo R'
7	'G_temp_sup-Plan_tempo L'	53	-19	6	1.5381	0.7255	1	1.3597	0.7373	53	-20	6	'G_temp_sup-Plan_tempo L'
8	'Lat_Fis-post L'	47	-23	11	0.6597	0.6980	5	0.7086	0.7039	50	-23	8	'S_temporal_transverse L'
9	'S_temporal_transverse R'	52	-32	16	1.1686	0.6999	0	0.8576	0.6586	52	-32	16	'G_temp_sup-Plan_tempo R'
10	'S_temporal_transverse R'	-57	-30	10	0.9994	0.7216	7	1.1710	0.7275	-54	-35	14	'G_temp_sup-G_T_transv R'
11	'Lat_Fis-post L'	-42	-33	9	0.6639	0.7137	16	0.3220	0.6370	-52	-22	4	'G_temp_sup-G_T_transv L'
12	'Lat_Fis-post L'	53	-20	6	1.9253	0.7058	7	1.6850	0.6980	56	-24	10	'G_temp_sup-Plan_tempo L'
13	'G_temp_sup-Plan_tempo R'	46	-26	10	0.4627	0.7019	7	0.4181	0.7098	41	-21	11	'G_temp_sup-Plan_tempo R'
14	'G_temp_sup-G_T_transv R'	-38	-32	16	0.7940	0.6901	21	0.7391	0.7117	-54	-20	8	'S_temporal_transverse R'
15	'Lat_Fis-post R'	-45	-38	16	0.3294	0.6232	29	0.3783	0.6272	-65	-19	5	'G_temp_sup-Plan_tempo R'
16	'S_temporal_transverse L'	54	-28	12	0.3882	0.6488	6	0.5173	0.6822	52	-32	16	'S_temporal_transverse L'